China Ocean Engineering, Vol.19, No.1, pp.37 – 48

Experimental Investigation of Wave Heights in A Directional Wave Field Through Image Sequences*

Chung-Ren CHOU[a], Teng-Wei LIN[a, 1], Ruey-Syan SHIH[b] and John Z. YIM[a]

[a] *Department of Harbor and River Engineering, National Taiwan Ocean University, Keeling 20299, China*

[b] *Department of Civil Engineering, Tung Nan Institute of Technology, Taipei 22202, China*

(Received 1 October 2004; accepted 20 December 2004)

ABSTRACT

Measurements of wave heights with image sequences from a Charged Coupled Device(CCD) camera were made. Sinusoidal, as well as unidirectional and directional, waves were used for the experiments. A transfer function was obtained by calibration of the magnitudes of the gray values of the images against the results of wave gauge measurements for directional waves. With this transfer function, wave heights for regular waves were deduced. It is shown that the average relative errors are smaller than 16% for both unidirectional and directional waves.

Key words: *charged coupled device; remote sensing; directional wave; transfer function; wave height measurements*

1. Introduction

Wave heights are usually measured by use of various types of wave gauges with fairly accurate results. However, there are some (rather severe) limitations associated with measurements with wave gauges. Because of their surface contacting nature, errors may occur as there are possible interactions between the waves, wave gauges and the props. This is especially true in laboratory, where all the experiments are to be carried out to reduced scales. When the spatial distribution of wave heights is to be studied, either a large number of wave gauges has to be deployed and measurements carried out simultaneously, or the wave gauge arrays have to be relocated with the same experiments repeated. Furthermore, wave gauges, together with their supports, may also obstruct such activities as navigation and fishing, and, as a result, there are reports upon measuring instruments torn down by angry fishers. It should also be mentioned that the deployment of surface contacting measuring devices may also be a problem. This is especially true for severe weather conditions, such as when there is a surge, rainstorm, hurricane or typhoon. It should also be pointed out that the results from these instruments are only point measurements, which are insufficient for the description of the whole wave field.

On the other hand, relatively large regions can be covered by use of remote sensing techniques. As a result of the advances in remote sensing techniques, a large amount of data can be collected instantaneously. The instruments can be mounted on an aircraft or installed on land with relative ease. This advantage will not only help increase the data collections for describing the wave field, but also

* This work was financially supported by the Science Council, Taiwan (Project No. NSC-91-2611-E-019-007)

1 Corresponding author. E-mail: m91520041@mail.ntou.edu.tw

reduce the extraneous expenses and labor cost.

There are various kinds of remote sensing techniques such as stereo-photography and radar system. The former contains two cameras positioned separately on airborne vehicles. Horikawa (1988) once mentioned that Horikawa *et al*. analyzed the wave spectrum, the wavelength and the wave direction by studying the stereographs taken simultaneously by two helicopters. Later, Sasaki *et al*. carried out similar experiments with photographs taken by two observation balloons. However, the experiments can be conducted only when the prevailing wind speed is smaller than 5 m/sec. Otherwise, the maneuvering of the balloons will be influenced. The radar system has long been adopted in sensing ocean wave fields. Marine-(X-band) radars were used by Gangerskar (2000) to observe ocean waves on the Gullfaks C drilling platform in the North Sea. He analyzed the influences of sea surface variations on the reflected signals of the radar. Using the relations between the effects and wave spectral parameters, he estimated the distributions of wave heights. The use of radar as an instrument for ocean wave observation has the clear advantage that a large area can be covered at one instant. However, it also has the disadvantage that reflections from wave troughs are often sheltered by prominent wave crests and this can lead to underestimation of wave heights. Other techniques such as satellites are also used for aerial survey.

In the earlier days, the signals reflected from the water surface can only be displayed either analogously on a radar screen, or picturesquely on the photographic paper. These "images" must be digitized afterwards. With the advance in the digital technique, digitized images can be obtained almost without any time delay. Referring to Gangerskar (2000), one can see that the strength of light reflections received by a camera or radar is affected by the slope of the water surface, not by the wave height.

In the study of water waves using numerous remote sensing techniques, the most difficult part is to establish a relation between the images obtained from the instruments and the actual motions of the water surface. In an attempt to resolve this problem, Chou *et al*. (2004) determined the hydrographic parameter of water surface from a sequence of images. A transfer function was obtained through comparison of the gray scale intensity with the actual wave height measured on site for regular waves in laboratory. They have shown that, when this relation is used for unidirectional waves, the average relative errors are smaller than 16%. However, further use of this relation for directional seas appeared unfavorable. This is probably due to the random variations in both temporal and spatial domains of the water surface for a directional wave field. Unlike the other two cases, the reflections from the water surface become inconspicuous for a directional sea. Water surface motions are more complicated due to the overlapping of waves propagating in various forms.

In this study, we carry out the studies of Chou *et al*. (2004) one step further. The motions of directional waves are filmed by a highly sensitive CCD camera. Through comparison of the magnitude of the gray scales obtained from the image sequences with the data measured by wave gauges, a transfer function is obtained. It is shown that this transfer function can be used to extract wave heights from the images of CCD camera.

2. Experiments and Data Processing

2.1 Experimental Setup

Experiments were carried out in the rectangular wave basin of 50 m by 50 m at the Ocean Engineering Laboratory of National Taiwan Ocean University. The segmented "serpentine wave generator" is composed of 56 piston-type paddles. The width of each paddle is 0.50 m, thus, the total length of the wave generator is 28 m. During the experiments, the water depth in the basin was 0.40 m. Theoretically, waves with a propagation angle between $0 \leqslant \theta \leqslant \pi$, θ denoting the main direction of the waves, can be generated. The optimal conditions are found to be $30° \leqslant \theta \leqslant 150°$, with periods between 0.5 ~ 5.0 sec, allowing the generation of a maximum wave height of 20 cm.

A total of 31 wave gauges of capacitance-type were used for the experiments. To measure the heights of the incident waves, a wave gauge was located at a distance of 4.3 m in front of the wave generator. As can be seen from Fig. 1, the remaining 30 wave gauges are arranged in a rectangular array. The long side of the array has 6, while the short side has 5, wave gauges, the spacing being 0.8 and 0.4 meters, respectively. The total area covered by the wave gauge array is thus 4×1.6 m^2. Results obtained from the wave gauges in this area will be used for comparison with those from CCD images, so that a transfer function between the magnitude of the gray value and the actual wave height can be derived. In the following, this area will be called Area-A. The 30 measuring stations of the array in the image are also shown in Fig. 1.

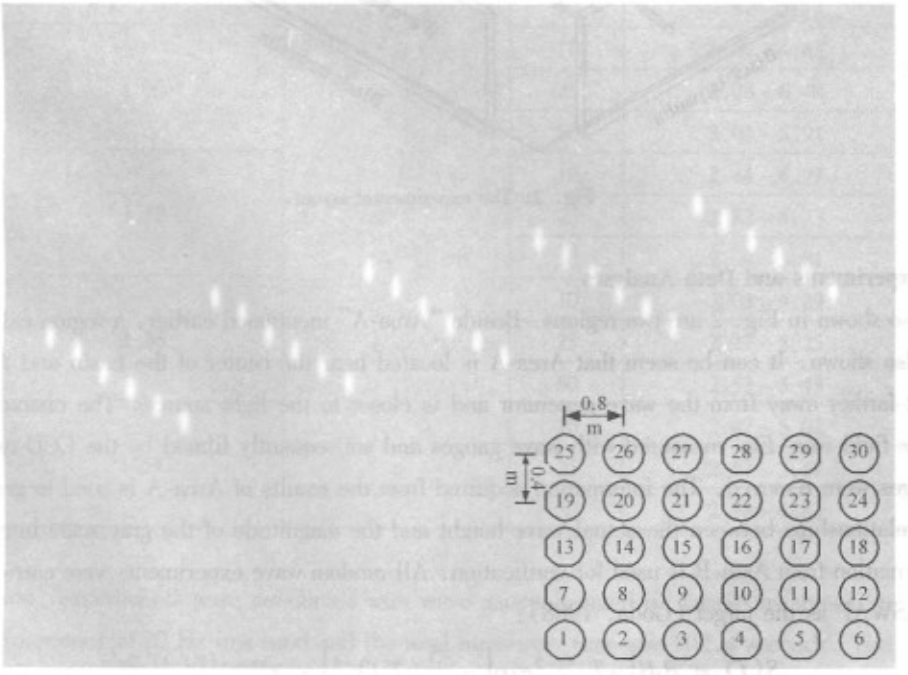

Fig. 1. Diagram for the wave gauge arrangement and locations of gauges in image.

Facing the wave generator, a highly sensitive CCD camera was located at the right-hand side aloft, and was 7.4 m away from the water surface. The camera could operate with light sources both in the visible and infrared ranges. A remote control device enabled the adjustment of the focal length, the filming angle, and the scope in the control room. The effects of scattered lights and reflection were minimized by polarizing the filter lens. The images were recorded in AVI format.

The experimental setup was similar to that of Chou *et al*. (2004). For the avoidance of reflections of the surroundings under daylight, the experiments were carried out at night. And in order to making the same background, the black tarpaulins were be set around the basin. Four 400-Watts light projectors were used as the light source. A more detailed description can be found in Chou *et al*. (2004). Fig. 2 is a sketch of the experimental setup.

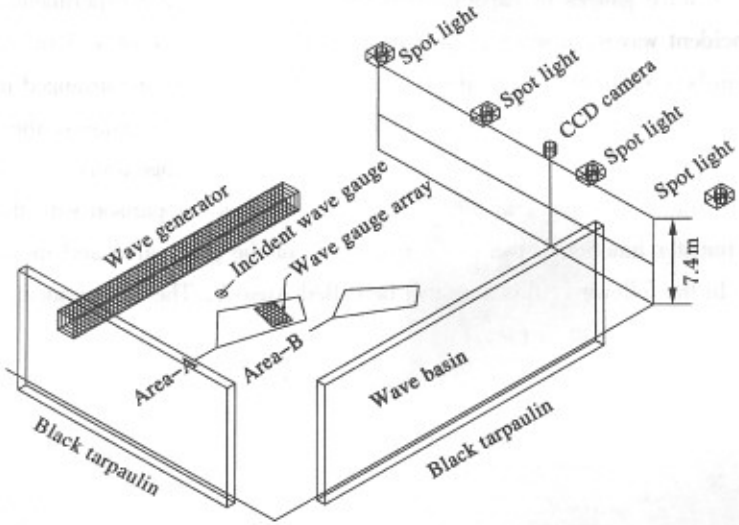

Fig. 2. The experimental layout.

2.2 Experiments and Data Analyses

Also shown in Fig. 2 are two regions. Beside "Area-A" mentioned earlier, a region called "Area-B" is also shown. It can be seem that Area-A is located near the center of the basin and Area-B is a little bit farther away from the wave generator and is closer to the light source. The characteristics of the wave field were first measured with wave gauges and subsequently filmed by the CCD camera after the gauges were removed. The information acquired from the results of Area-A is used to generate empirical relationships between the actual wave height and the magnitude of the gray scale intensity, and the information from Area-B is used for verification. All random wave experiments were carried out with the JONSWAP as the target (Goda, 1988):

$$S(f) = \beta_J H_{1/3}^2 T_p^{-4} f^{-5} \exp\left[-\frac{5}{4}(T_p f)^{-4}\right] \times \gamma^{\exp[-(T_p f-1)^2/2\sigma^2]} \quad (1)$$

with

$$\beta_J = \frac{0.0624}{0.230 + 0.0336\gamma - 0.185(1.9 + \gamma)^{-1}}[1.094 - 0.01915\ln\gamma],$$

$$T_p \simeq T_{1/3}/[1 - 0.132(\gamma + 0.2)^{-0.559}], \text{ and}$$

$$\sigma = \begin{cases} 0.07 & f \leqslant f_p; \\ 0.09 & f > f_p; \end{cases}$$

where $H_{1/3}$, $T_{1/3}$, T_p, f_p, and γ (mean ≈ 3.3) are, respectively, the significant wave height, the significant wave period, the spectral peak period, the peak frequency, and the peak enhancement factor.

Random waves with peak frequencies of 0.95, 1.06, 1.19, 1.36, and 1.59 Hz were chosen for the experiments. To model different sea states, three spreading indexes (Goda, 2000), S_{max}, with values equal to 10, 25, and 50 were used for each of the peak frequency to generate directional waves. The wave heights were approximately in the range of 1.81 to 6.48 cm. The experimental conditions are shown in Table 1.

Table 1 The experimental conditions for directional waves

Peak frequency (Hz)	Peak direction θ	S_{max}	Wave height $H_{1/3}$ (cm)
0.95	90°	10	2.07 ~ 4.89
		25	2.60 ~ 5.50
		50	2.81 ~ 5.77
1.06		10	1.81 ~ 4.45
		25	2.78 ~ 6.48
		50	3.01 ~ 5.91
1.19		10	2.44 ~ 4.92
		25	2.82 ~ 5.73
		50	2.94 ~ 5.81
1.36		10	2.03 ~ 4.29
		25	2.37 ~ 5.25
		50	2.53 ~ 5.43
1.59		10	2.47 ~ 5.02
		25	2.67 ~ 5.17
		50	2.58 ~ 4.83

At first, experiments were conducted with wave gauges located in Area-A as shown in Fig. 2. A sampling frequency of 20 Hz was used and the total measuring time was 102.4 seconds. The significant wave heights ($H_{1/3}$) as well as the significant wave periods ($T_{1/3}$) were obtained through zero-down-crossing. To be comparable with wave gauge results, video images were also digitized with a rate of 20 frames per second.

Throughout the experiments, the video images were recorded in monochrome format. All colors were therefore expressed as gray values in the digitized image in the range of 0 ~ 255. The color white is the brightest in the image and has a gray scale value of 255, whereas the color black is the darkest and has a value of 0. All the raw images have a resolution of 320 × 240 pixels. However, as pointed out by Jähne (1997), electronic noises, non-uniformity of the illumination, as well as inhomogeneities of the background often contaminate the resolution of the raw image. For minimization of the effect of noise contamination, the images were smoothed in two steps. At first, the averaged values of the gray scales for the measuring stations were obtained. This was done by averaging the values of the gray scales of four adjacent pixels, as sketched in Fig. 3a. A new image with 160 by 120 pixels then resulted. The points corresponding to the locations of the wave gauges were then chosen from the smoothed images. A further step of smoothing was achieved in such a way that the gray scales of the chosen points in the images were further averaged with those of their eight surrounding pixels. In the following, we will call this procedure "using a 3 by 3 box-filter".

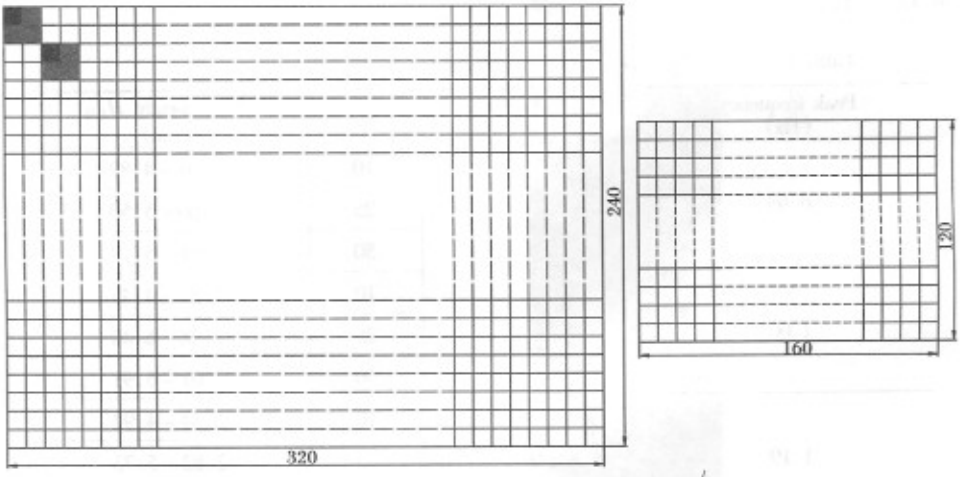

$$\eta_{(i,j)} = \left(\eta_{(i,j)} + \eta_{(i+1,j)} + \eta_{(i+1,j+1)} + \eta_{(i,j+1)}\right) \Big/ 4$$

(a) the 2 by 2 smooth-screen

$\eta(x-1,y-1)$	$\eta(x,y-1)$	$\eta(x+1,y-1)$
$\eta(x-1,y)$	$\eta(x,y)$	$\eta(x+1,y)$
$\eta(x-1,y+1)$	$\eta(x,y+1)$	$\eta(x+1,y+1)$

$$\eta'(x,y) = \begin{bmatrix} 0.5 \times \eta(x-1,y-1) + \eta(x,y-1) + 0.5 \times \eta(x+1,y-1) \\ + \eta(x-1,y) + 2 \times \eta(x,y) + \eta(x+1,y) \\ + 0.5 \times \eta(x-1,y+1) + \eta(x,y+1) + 0.5 \times \eta(x+1,y+1) \end{bmatrix} \Big/ 8$$

(b) the 3 by 3 box-filter

Fig. 3. The smoothing process in the spatial domain.

The time series of gray scale variations of the measuring stations can then be obtained from the

image sequences. In the time domain, the image sequences of the measuring stations are further smoothed with a 5-point running average of the form:

$$\eta_t = (-\eta_{t-2} + 4\eta_{t-1} + 10\eta_t + 4\eta_{t+1} - \eta_{t+2})/16 \quad (2)$$

where η_t denotes the gray scale at time t, and $t+1$ and $t-1$ have the meaning of, respectively, one-step prior to or later than the present time t.

From the time series of gray scale fluctuations, a mean gray value, denoted as G_{AVG}, can be defined. This value is an index for the strength of the illumination. This corresponds to the mean water level of the time series of surface fluctuations. After subtraction of this mean value, the method of zero-downcrossing can be applied.

As done for the time series of water surface fluctuations, from each time series of the gray scale fluctuations, a (significant) gray magnitude, $G_{1/3}$, and its associated gray period, $T_{G1/3}$, can be obtained. These will then be compared with those measured by the wave gauges for the derivation of the transfer function that will be needed later on.

3. Results and Discussion

Jähne and Riemer (1990) pointed out that the lights reflected from the water surface depend on the light intensity it received. They further pointed out that, the intensities of the gray values of the images will decrease with increasing distances away from the light source. The same facts were also found by Chou *et al.* (2004, 2003) in their studies of sinusoidal and unidirectional waves using a CCD camera, and they expected that the effects of light source inhomogeneity should be reduced. With the average of all of the gray magnitudes denoted as G_m, this then corresponds to the mean wave height for the wave basin measured by the wave gauges. Referring to Chou *et al.* (2003), one can find that the value of G_m decreases with the increasing value of G_{AVG}. This, however, is not seen in our experiments with directional waves. In order to compare that, we re-tested their experimental conditions again which are shown in Table 2 and Table 3.

Table 2 The experimental conditions for unidirectional waves

Direction θ	90°				
Peak frequency f(Hz)	0.95	1.06	1.19	1.36	1.59
Wave height $H_{1/3}$ (cm)	2.07 ~ 4.89	1.81 ~ 4.45	2.44 ~ 4.92	2.03 ~ 4.29	2.47 ~ 5.02

Table 3 The experimental conditions of sinusoidal waves

Direction θ	90°				
Period T (sec)	0.6	0.7	0.8	0.9	1.0
Wave height H(cm)	2.64 ~ 5.70	3.42 ~ 6.74	3.30 ~ 6.74	3.41 ~ 6.42	3.10 ~ 5.25

From the study with sinusoidal waves, Chou *et al*. (2004) derived a transfer function between the wave height and the "gray magnitude". The relative errors between estimated and measured wave heights are smaller than 16% when this transfer function is applied to unidirectional waves; however, when this transfer function is used for directional waves, the results are less satisfactory.

The reason for the lack of agreement for directional waves may be explained as follows. For sinusoidal and directional waves, the wave crests are continuous across the basin—they are therefore known as long-crested waves. Even though the light intensities at the far end of the basin are lower than at the near side, the relative strength of the illumination remains approximately the same as wave crests and troughs pass through the frame. Fig. 4 is an image from sinusoidal wave experiments, where the waves have a period of 0.6 sec and the wave height is about 0.05 m. As the crests are higher than the still water surface, they receive more lights, and are therefore brighter than their surroundings. They are thus clearly seen as the bright strips across the frame.

On the other hand, for directional waves, the wave crests are discontinuous and unorganized. Thus, there will be no distinct crest lines on the water surface, as can be seen from Fig. 5, which was taken during one of the directional wave experiments. To be comparable with the sinusoidal wave experiment shown in Fig. 6, the short-crested waves were generated with corresponding conditions. That is, they had a significant wave period, $T_{1/3}$, of 0.6 sec, and a significant wave height, $H_{1/3}$, of 0.05 m. The spreading index, S_{max}, of these waves is 50. In this case, the gray scales of the images do not have a clear contrast like for unidirectional waves.

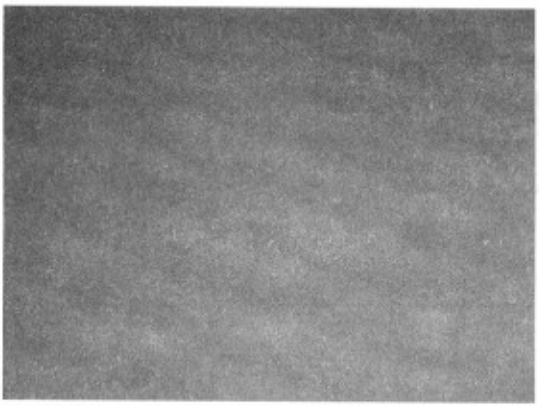

Fig. 4. An image of the sinusoidal wave with $T = 0.6$ sec and $H = 5$ cm.

Fig. 5. An image of the directional wave with $T_{1/3} = 0.6$ sec, $S_{max} = 50$, and $H_{1/3} = 5$ cm.

Therefore, we can go a step further to explain Figs. 6a ~ 6d. These figures show the relationships between G_{AVG} and G_m. For the expression of the difference between the values of each measuring point, the value of G_m was offset by multiplying a factor of 10. Figs. 6a ~ 6b show these relations for the measuring points of Nos. 1, 6, 11, 16, 21, and 26 for regular and directional waves, respectively, and Figs. 6c ~ 6d are for Nos. 3, 8, 13, 18, 23, and 28. Their respective locations can be seen from Fig. 1. The measuring point of No. 1 was the nearest to the light in this cross-section, whereas

No. 26 was the farthest. It is easy to see that the value of G_m seems to be inversely proportional to the value of G_{AVG} in Fig. 6a, and the same trend can be detected from Fig. 6c. But from Figs. 6b and 6d, no definite relationships can be found between the values of G_{AVG} and G_m. It is therefore considered that it is not necessary to modify the value of G_m for directional waves.

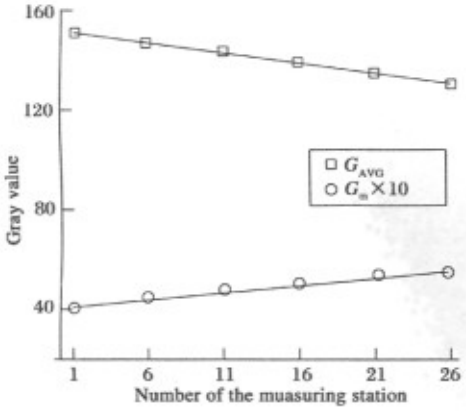

Fig. 6a. The relationships between G_{AVG} and G_m for sinusoidal waves for the measuring stations of Nos. 1, 6, 11, 16, 21, and 26.

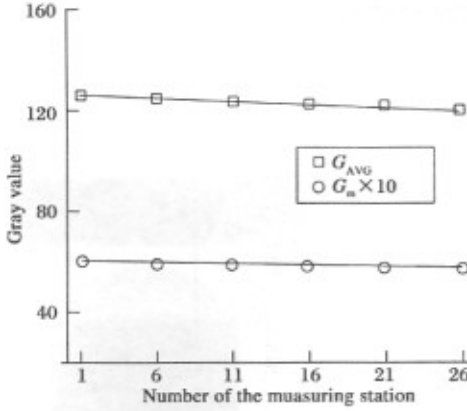

Fig. 6b. The relationships between G_{AVG} and G_m for directional waves for the measuring stations of Nos. 1, 6, 11, 16, 21, and 26.

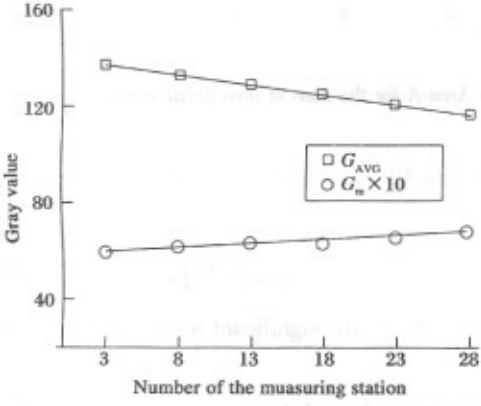

Fig. 6c. The relationships between G_{AVG} and G_m for sinusoidal waves for the measuring stations of Nos. 3, 8, 13, 18, 23, and 28.

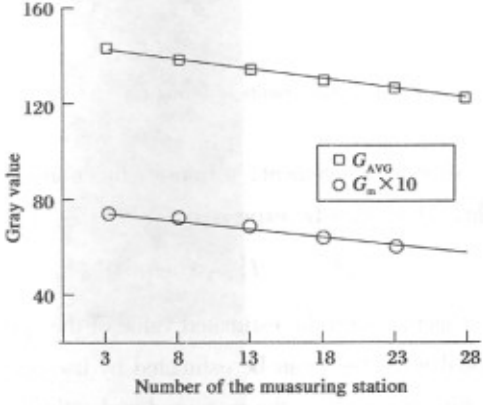

Fig. 6d. The relationships between G_{AVG} and G_m for directional waves for the measuring stations of Nos. 3, 8, 13, 18, 23, and 28.

With periods estimated from image sequences, wavelengths can be obtained with the dispersion relation for small amplitude waves:

$$\sigma^2 = gh\tanh kh; \quad \sigma = 2\pi/T; \quad k = 2\pi/T. \tag{3}$$

After some adjustments, a regression line can be drawn for the results shown in Fig. 7:

$$\ln\left(\frac{H_{1/3}}{L_{G1/3}}\right)\cdot\frac{1}{\sqrt[3]{\ln(S_{\max})}}\cdot(T_{G1/3})^{1.218}=0.2463\cdot\sqrt{G_{1/3}} \tag{4}$$

where $H_{1/3}$ is the significant wave height measured by the wave gauges (in centimeters); $S_{\max}$ is the spreading index; $T_{G1/3}$ is the gray period; $L_{G1/3}$ is the wavelength calculated with $T_{G1/3}$; $G_{1/3}$ is the gray magnitude.

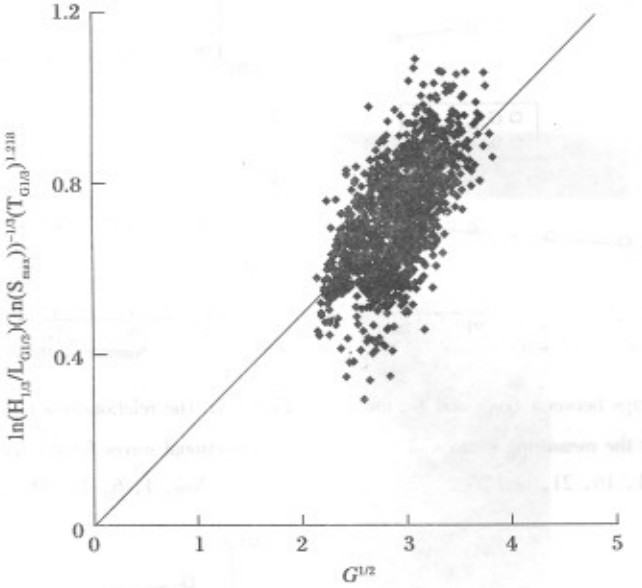

Fig. 7. The results of fitting Eq. (5) for the data from Area-A for the case of directional waves.

After rearrangement, a transfer function is finally obtained between the gray magnitude and wave height, which can be expressed as:

$$\dot{H}_{1/3}=L_{G1/3}\cdot\exp\left[0.2463\cdot\sqrt{G_{1/3}}\cdot\sqrt[3]{\ln(S_{\max})}\Big/(T_{G1/3})^{1.218}\right]. \tag{5}$$

Together with the estimated value of the spreading index $S_{\max}$, the significant wave height of a directional wave field can be estimated by use of Eq. (5).

Fig. 8 compares the measured and estimated wave heights in Area-A for a directional wave field. Each symbol in the figure denotes the averaged value of the 30 measuring stations for the same experimental condition. It can be seen from the figure that all the symbols are distributed over a straight line, indicating the equality of the estimated and measured wave heights. The average of the relative errors for Area-A is about 17% for directional waves, where the relative error is defined as:

$$\text{err}=\left|H_{\text{estimated}}-H_{\text{measured}}\right|/H_{\text{measured}} \tag{6}$$

where H_{measured} and $H_{\text{estimated}}$ are, respectively, the wave height from wave gauge measurement and that estimated from image sequences.

This transfer function was then tested against Area-B. It was found that, for directional waves, the average of relative errors is about 16.96%. It can be seen from Fig. 9 that, in general, the wave

heights estimated from images are somewhat larger than those measured by the wave gauges. The differences are, however, not large. This is considered to demonstrate that the transfer function can be used for other areas of the basin.

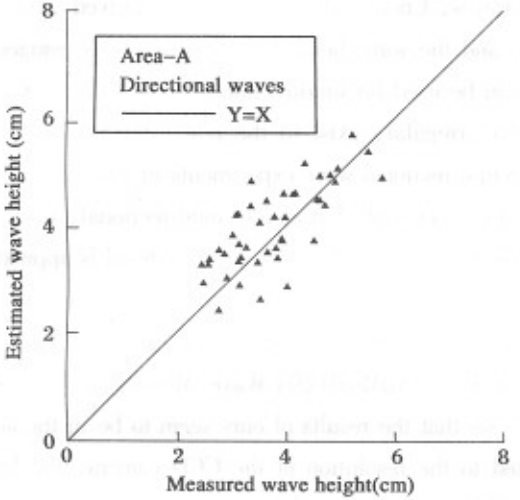

Fig. 8. Comparison of estimated and measured wave heights within Area-A.

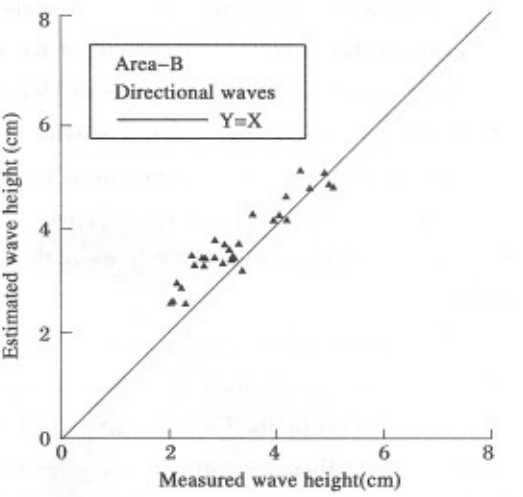

Fig. 9. Comparison of estimated and measured wave heights within Area-B.

Therefore, the values of the relative errors for wave heights are within 17% for both Area-A and Area-B for directional waves. The transfer function is then tested against unidirectional waves. We have used 0.95, 1.06, 1.19, 1.36, and 1.59 Hz as the peak frequencies of unidirectional waves. For each peak frequency, we have used four different significant wave heights in the range of 2.03 to 5.02 cm. As for sinusoidal waves, waves with periods of 0.6, 0.7, 0.8, 0.9, and 1.0 sec, each with six different wave heights in the range of 2.64 to 6.74 cm, are used. Tables 2 and 3 list the experimental conditions. If a value of 75 for the spreading index S_{max} is used for both cases, the relative errors can then be estimated. It is found that, the relative error for unidirectional waves is 9.48%, while it is 17.39% for sinusoidal waves.

Chou *et al.* (2004) found that removing the points on the far end of the image plan leads to better results. The illumination for these points is insufficient, and is considered to have a negative effect on the overall results. Following their method, we have chosen from the image the points 7 to 9, 12 to 14, and 22 to 24 for the analysis. A new transfer function is obtained:

$$H_{1/3} = L_{G1/3} \cdot \exp\left[0.2091 \cdot \sqrt{G_{1/3}} \cdot \sqrt[3]{\ln(S_{max})}/(T_{G1/3})^{1.636}\right]. \quad (7)$$

It is found that, with this new transfer function, the relative errors for directional waves are, respectively, 15.2% and 15.4% for Area-A and Area-B. However, when this transfer function is used for unidirectional and sinusoidal waves, the relative errors for Area-B become larger.

4. Conclusions

In this study, developed is a measuring system in which a CCD camera is used to sense the wave

weight. A series of experiments indicates that the system is feasible for small-scale experiments. In addition, it must be stressed that further studies are necessary before the present technique can be used for field experiments.

Using the data from experiments with sinusoidal waves, Chou *et al*. (2004) have derived a transfer function between the gray magnitude of the image and the wave height measured by wave gauges. They have further shown that their transfer function can be used for unidirectional waves. However, it is well known that no unidirectional waves, regular or irregular, exist in the real world. We have, therefore, derived a transfer function using the data from directional wave experiments in this study. As verification, this transfer function is applied not only to directional, but also to unidirectional, waves. It is shown that the overall relative error of this transfer function for all the cases considered is approximately 16%.

A comparison of our relative error with the error of previous researches, such as Jähne and Schults (1992) (21%) or commercial measuring systems such as WaMoSII® (Wave Monitoring System) (10%) developed by the German GKSS institute, shows that the results of ours seem to be in the acceptable range. Therefore, the relative error is related to the resolution of the CCD camera, the low resolution resulting in the increase of the error. In the future, higher resolution cameras may help solve this problem.

Compared with conventional methods, a CCD camera has the advantage of acquiring the information of the whole wave field at one instant. Furthermore, it can be mounted with relative ease. The validity and accuracy of the methods have been verified by comparison with the results of the in-situ measurements of wave gauges. This technique is promising.

References

Chou, C. R., Yim, J. Z. and Huang, W. P., 2004. Determining the hydrographic parameters of the water surface from image sequences of CCD camera, *Experiments in Fluids*, **36**(4): 515 ~ 527.

Chou, C. R., Yim, J. Z. and Huang, W. P., 2003. Sensing water surface fluctuations through CCD image sequence, *J. of Coastal and Ocean Eng.*, Taiwan Society of Ocean Engineering, **3**(1): 53 ~ 71. (in Chinese)

Gangeskar, R., 2000. Wave height derived by texture analysis of X-band radar sea surface image, *Proceedings*, *IGARSS 2000*, IEEE, Vol. 7, 2952 ~ 2959.

Goda, Y., 1988. Statistical variability of sea state parameters as function of wave spectrum, *Coastal Engineering in Japan*, JSCE, **31**(1): 39 ~ 52.

Goda, Y., 2000. *Random seas and design of maritime structures* (2nd Edition), World Scientific, Singapore, 12 ~ 43.

Horikawa, K., 1988. *Nearshore dynamics and costal processes*, University of Tokyo Press, 399 ~ 401.

Jähne, B. and Riemer, K. S., 1990. Two-dimensional wave number spectra of small-scale water surface waves, *J. of Geophys. Res.*, **95**(D5): 11531 ~ 11546.

Jähne, B. and Schults, H., 1992. Calibration and accuracy of optical slope measurement for short wind waves, in: Optics of the Air-Sea Interface: Theory and Measurement, Leland, E. ed., *Proc. SPIE* Vol. 1749, 222 ~ 233.

Jähne, B., 1997. *Digital image processing*, Springer-Verlag, Berlin, 289 ~ 341.

WaMoSII®: Technical data sheet and system requirement & benefits [online], available from World Wide Web: < http://www.oceanwaves.de/technicals.htm >